Energy shifts and broadening of atomic levels near metal surfaces

P. Nordlander
Department of Physics, Rice University, P.O. Box 1892, Houston, Texas 77251-1892

J. C. Tully
AT&T Bell Laboratories, Murray Hill, New Jersey 07974-2070
(Received 7 August 1989; revised manuscript received 16 April 1990)

We present calculations of the lifetime broadening and the shifts of hydrogenlike atomic levels (ground and excited states of H, Li, Na, K, Rb, and Cs) near jellium metal surfaces (Al and Na). The energies and widths of the atomic resonances are obtained from the Schrödinger equation with use of the complex scaling technique; the electron potential in the surface region is calculated with use of density-functional theory. We find that the energy shifts of the atomic levels are influenced mainly by the properties of the surface potential close to the atom. The widths of the atomic levels, on the other hand, depend on the surface potential in the whole surface region. We show that in order to obtain accurate widths of atomic levels it is important to incorporate nonlocal effects, particularly the image potential. We also find that the widths are strongly influenced by hybridization among the near-degenerate atomic levels. The excited atomic levels shift differently with distance from the surface leading to multiple level crossings. At such positions the hybridization can be strongly enhanced, resulting in states that are oriented towards or away from the surface, with very different lifetimes that may vary in a nonexponential manner with distance from the surface.

I. INTRODUCTION

The energies and lifetimes of excited states of atoms and molecules at or near solid surfaces are controlling factors in many physical phenomena. For example, electron or photon radiation can stimulate desorption of surface atoms if electronically excited repulsive states are localized and sufficiently long lived.[1,2] Furthermore, the final charge and electronic states of the species so produced will be influenced by the lifetimes of the competing levels and the curve crossings they exhibit.[3] Photochemistry at surfaces depends on the enhanced reactivity of electronically excited species and the time the excitation survives.[4] The angular, velocity, charge, and electronic-state distributions of sputtered particles depend strongly on the lifetimes of the electronic states.[5] In the spectroscopy of adsorbed species, the lifetimes of excited states contribute to the broadening of adsorption peaks.[6-8] Finally, the lifetimes and energies of excited states determine the survival probabilities of excited species in the scattering of atoms and molecules from surfaces.[9-11]

Charge-transfer processes at surfaces are usually described with use of dynamical theories based on the Anderson Hamiltonian.[12-14] The energy shifts and lifetimes of the excited states are crucial parameters in such models. In particular, the final state of a scattered atom can be strongly influenced by transitions that occur near the positions where the energy of the atomic state becomes resonant with the Fermi energy of the metal. Such crossings can occur at large atom-surface separations, so in order to obtain a complete description of charge transfer it is necessary to obtain the energy shifts and lifetimes of the levels for a broad range of distances from the surface.

In spite of the obvious importance of the dynamics of excited adsorbate states there is relatively little known either theoretically or experimentally about how excited states shift and decay at surfaces. There are many reasons for this. From a theoretical standpoint, calculations of excited-state properties are difficult. Density-functional theories are questionable for the description of excited states.[15,16] The conventional many-body theory that is used for electronic-structure calculations at surfaces, the local-density approximation (LDA), is valid only for small adsorbate-substrate separations and does not apply to all distances of interest in typical atom-surface dynamical processes. Furthermore, due to coupling to the metal conduction band, excited states are associated with resonant scattering wave functions that are not square integrable. Conventional bound-state techniques are, therefore, not applicable and scattering techniques must be used.

From an experimental point of view, until very recently there have been no techniques that can provide direct measurements of lifetimes of excited adsorbate states. Traditionally, lifetimes have been estimated by linewidth analysis. There can, however, be other contributions to the broadening of spectral features that have nothing to do with the lifetime of the state and may dominate the observed width. Recently the first direct measurements of excited electronic-state lifetimes at surfaces have been performed using time-resolved techniques.[17,18] With the further development and refinement of ultrashort laser-pulse techniques it is likely that such real-time measurements will be able to provide detailed information about lifetimes of excited states at surfaces.

While at present there exists no simple computational technique to calculate the total energy of an excited atom

at a metal surface, it is less difficult to calculate energy shifts and lifetimes of individual valence levels of adsorbates at relatively large distances from the surface (more than 5 a.u.). This is because the dominant contribution to the lifetimes of the excited states at such distances is resonant tunneling of electrons between the adsorbate level and the surface.[19] The tunneling rates are determined by the variation of the electron potential in the region separating the adsorbate from the surface. The electron potential outside a metal surface is a relatively well-known quantity that can be calculated theoretically[20–22] and can also be probed experimentally, for instance, by low-energy electron diffraction techniques.[23]

There have been several theoretical calculations of the shifts and broadening of atomic levels at chemisorption distances from surfaces[24–26] but relatively few for the larger distances relevant for scattering or desorption processes. Gurney[27] calculated the shifts of atomic levels outside a perfectly conducting metal surface. Gadzuk[28] and Remy[29] calculated the shifts and also the broadening of the ionization levels of the alkali atoms outside metal surfaces. Both of these studies used perturbation theory, and employed an idealized surface potential. The widths of the adsorbate resonances, in particular, are sensitive to the details of the surface potential, and it is important to represent this function accurately. A more sophisticated approach to evaluate the width of atomic states outside a metal surface was taken by Grozdanov and Janev[30] who used a WKB approach to evaluate the tunneling rates. These authors, however, used an electron potential that diverges at the surface. In order to obtain tractable solutions, they introduced parabolic coordinates with the result that the surface plane was implicitly curved towards the adsorbate. The combination of inaccurate potential and curved surface plane resulted in calculated level widths that are too large.[31] Another shortcoming of all of these studies is that the hybridization of atomic levels was not properly taken into account. As we will show below, the mixing of nearly degenerate atomic states can have a drastic effect on level widths.

In this paper we present a calculation of the shifts and broadening of atomic levels in the vicinity of a metal surface. We calculate the level shifts and widths directly from the density-functional surface potential using the nonperturbative "complex-scaling" method.[32] The adsorbate states are allowed to hybridize and mix with the electronic states of the surface. We consider adsorbates at physisorption distances from the surface (distances larger than 5 a.u. from the surface). At such distances the adsorbate-metal interaction can be adequately modeled using the jellium description of the metal surface. The jellium model represents the potential due to the positive ion cores in a metal by a smeared out constant attractive potential.[33] The potential thus has no lateral variation but increases steeply to zero away from the surface. The jellium model is appropriate for large adsorbate-surface separations because the effects of lateral corrugation of the metal surface decay rapidly with distance from the surface.[34] The present application is restricted to a one-electron description of the adsorbate atomic levels. This assumption is reasonable for describing the excited states of hydrogen and alkali atoms. In Sec. II, we present the theoretical details of the calculation. In Sec. III the results of the calculations are presented. In Sec. IV we present a discussion of how the surface potential influences the calculated shifts and level widths. In Sec. V we discuss some limitations and possible extensions. In Sec. VI we present the conclusions of the paper.

II. THEORY

In this section we outline the method of calculation. As will be elaborated upon below, the lifetimes of the atomic states can be obtained directly from the one-electron potential outside the surface. In Sec. II A we show how we construct this surface potential and in Sec. II B we describe a method for solving for the resulting resonance states. In the Appendix we give further details about the method.

A. The surface potential

When an atom is placed outside a metal surface, the atomic levels will shift in energy. The levels can also acquire widths, i.e., broaden into resonances. The energies of atomic states shift because the potential around the atom is altered. The broadening of atomic states is due to the continuum of surface electronic states into or out of which the electrons can tunnel. In general, the farther away from the surface an atom is, the smaller the tunneling probability because both the height and the breadth of the tunneling barrier increases.

The surface potential is a function of both electron and adsorbate coordinates. We use lower case letters to denote electron coordinates (ρ,z) and capital letters to denote atomic positions (Z). The z axis is directed outward from the surface and measured from the surface (jellium edge). The coordinate ρ indicates the radial distance along the surface from the surface normal through the atom. Unless otherwise indicated, atomic units will be used throughout the text. Thus distances are given in terms of the Bohr radius and energies in hartrees. We start by describing the interaction of an adsorbate with a perfectly conducting metal surface. We then describe how this interaction is modified when the surface is modeled using the jellium description.

Consider a positive ion at a fixed distance Z from a perfectly conducting metal surface. The resulting potential experienced by an electron is

$$V^{\text{eff}}(\rho,z;Z)=V_0^s(z)+\Delta V^s(\rho,z;Z)+V^A(\rho,z;Z)\ . \qquad (2.1)$$

The first term in Eq. (1) is the electron-surface interaction, $V_0^s(z)$, in the absence of the positive ion, which for a perfect conductor is just the image attraction, $-1/4z$. The second term $\Delta V^s(\rho,z;Z)$ is the change in the electron-surface potential induced by the positive ion, which for a perfect conductor is $[(z+Z)^2+\rho^2]^{-1/2}$, the repulsion between the electron and the negative charge induced in the surface due to the positive ion image. The third term $V^A(\rho,z;Z)$ is the direct electron-ion interaction, which for a proton is just $-1/r$; i.e.,

$[(z-Z)^2+\rho^2]^{-1/2}$. Thus for a hydrogen atom outside a perfect conductor, Eq. (2.1) becomes

$$V^{\text{eff}}(\rho,z;Z)=-\frac{1}{4z}+\frac{1}{[(z+Z)^2+\rho^2]^{1/2}}-\frac{1}{[(z-Z)^2+\rho^2]^{1/2}}\ . \tag{2.2}$$

The total potential for a neutral atom near a metal surface contains one additional term, the attractive interaction of the positive ion core with the surface, which for a proton near a perfect conductor is the attractive image potential $-1/4z$. This term does not affect the ionization energies or lifetimes of electronic levels, the quantities we calculate here, and so it is neglected in Eq. (2.1). It would need to be included to calculate total interaction energies of atoms with surfaces.

Figure 1(a) shows the first two terms of Eq. (2.1) for a perfectly conducting surface. The dashed curve is the electron-surface potential $V_0^s(z)$, i.e., $-1/4z$. The dotted curve is $\Delta V^s(\rho,z;Z)=[(z+Z)^2+\rho^2]^{-1/2}$ for a positive ion fixed at a distance $Z=10a_0$ from the surface. The solid curve is the sum $V_0^s+\Delta V^s$; i.e., the total electron potential excluding the direct electron-ion interaction. Note that even with this simple classical potential a potential energy barrier between the surface and the atom arises (solid curve). This barrier will reduce electron tunneling rates considerably. In addition, the sum of the electron-electron image and electron-core image interactions at a point very near the ion core is a net repulsive interaction of magnitude $1/4z$. This results in an upward shift of the electron levels with a corresponding reduction of the ionization potential. This upward shift of an electron level should not be confused with a total interaction potential. The attractive interaction between the core and the image core [neglected in Eq. (2.1) as discussed above] compensates for the shift in the electron level and the total static interaction potential approaches zero for a neutral atom at large distances. Due to the image charges, the adsorbate orbitals become slightly polarized and an attractive interaction results. This is the van der Waals interaction and its magnitude decays as Z^{-3}.

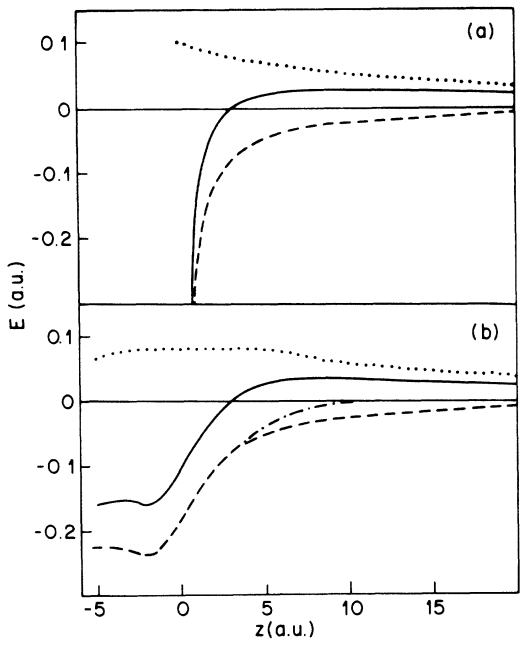

FIG. 1. In (a) we show the surface potential outside a perfectly conducting metal surface. The dashed line is the bare surface electron potential. The dotted line is the electron-core image potential for a proton placed at a distance $Z=10$, and $\rho=0$. The total potential is drawn with the solid line. In (b) we show the surface potential outside a realistic metal surface (jellium approximation with $r_s=2$). The dashed line is the bare surface potential calculated using density-functional theory. For comparison, the bare surface potential as obtained using the local-density approximation as also plotted (dashed-dotted line). The dotted line is the proton induced image potential. The solid line is the total density-functional potential.

For the interaction of an affinity level of an atom (i.e., a negative ion state) and a perfectly conducting surface the situation is very different. The core of the atom is neutral and there is no electron-core image repulsion. In this case, the affinity level shifts down by the electron-electron image interaction. Affinity levels therefore follow the surface potential and become stabilized at surfaces. Since there is no electron-core image barrier to prevent tunneling between the surface and the atom, affinity levels can be very broad.

The image approximations to $V_0^s(z)$ and $\Delta V^s(\rho,z;Z)$, Eq. (2.1), are not adequate for small or intermediate values of z. The image approximation to $V_0^s(z)$ diverges at small z, whereas the true potential should approach that of the bulk. In order to more accurately represent these potentials, we invoke the usual jellium approximation for the surface. We employ for $V_0^s(z)$ the density-functional (DF) electron-surface potential computed by Ossicini *et al.*,[20] employing the "weighted density approximation" suggested by Gunnarsson *et al.*[35] Alternative density-functional calculations of $V_0^s(z)$ have been reported.[36,37] These are quantitatively very similar to the Ossicini potential we have employed, and the use of one of these alternatives would have had essentially no influence on our results. All of these potentials correctly approach the image potential at large z, and smoothly approach the bulk potential for negative z, as shown by the dashed curve of Fig. 1(b). In contrast, potentials calculated by the conventional local-density approximation (LDA) are not adequate because they do not approach the image potential at large z. The LDA assumes that the exchange-correlation part of the electron potential at a point is determined by the local electron density at that point. This approximation neglects nonlocal interactions such as the image force, and is, therefore, valid only close to the surface. The difference between LDA and DF is significant and gives rise to marked differences in the level broadening at physisorption distances from the surface. In Sec. IV these differences will be discussed further.

In Fig. 1(b) we plot the LDA and the DF electron potentials outside a jellium surface. The potentials for the bare surface look very different from those in Fig. 1(a). The major reason for this is that the conductivity of a real surface is finite and the surface charges will be distri-

buted in a thin region around the selvedge.[38] At large distances from the surface the DF potential is imagelike. The potential is slightly changed compared to the perfectly conducting surface in Fig. 1(a) and has the form $\frac{1}{4}/(z-z_0)$, where z_0 is an effective image plane located at the center of gravity of the induced surface-charge distribution. The values of z_0 typically lie slightly outside the surface.[38] In contrast, the LDA surface potential vanishes exponentially outside the surface and there is no image contribution.

At a closer distance, the electron starts to overlap with the surface-electron density. As a result the electron is not entirely separated from its exchange-correlation hole and the image potential saturates close to the surface. In this region the surface potential also contains an electrostatic dipole contribution, that arises from the fact that the electron distribution is spread out around the selvedge. At these smaller distances the differences between LDA and DF become negligible.

The image approximation for the ion-induced potential $\Delta V^s(\rho,z;Z)$ is also adequate. The proton induces a negative image charge distribution in the selvedge. This charge distribution will give rise to both an electrostatic potential outside the surface (electron-core image repulsion) and also change the exchange-correlation potential close to the jellium edge. Thus

$$\Delta V^s(\rho,z;Z)=\Delta V^{el}(\rho,z;Z) \ . \tag{2.3}$$

We approximate the induced surface charge distribution responsible for the first term of Eq. (2.2) with a smeared surface charge density

$$\sigma(\rho',z',Z)=\frac{1}{\sqrt{\Delta}}e^{-(z'/\Delta)^2}\sigma_{\rm cl}(\rho',Z-z_0) \tag{2.4}$$

where $\sigma_{\rm cl}$ is the classical surface charge electron density for an infinitely conducting metal with a proton at distance $Z-z_0$ from the surface. z' is the distance from the image plane, Δ is the thickness of the surface charge distribution, and ρ' is the radial distance from the surface normal. The change in the electrostatic part of ΔV^s is then evaluated using Poisson's equation:

$$\Delta V^{el}(\rho,z,Z)=\int \frac{dz'}{\sqrt{\Delta}}e^{-(z'/\Delta)^2}\frac{1}{[\rho^2+(Z+z-z')^2]^{1/2}} \ . \tag{2.5}$$

The image charges are induced close to the surface, where the nonlocal exchange-correlation potential closely resembles the LDA result. We can therefore use the LDA methodology[38] and parameters to calculate the change in the exchange-correlation part of the surface potential $\Delta V^{\rm xc}$. Thus we employ the local-density expression

$$\Delta V^{\rm xc}(\rho,z,Z)=\mu^{\rm xc}[n_0(z)+\sigma(\rho,z,Z)]-\mu^{\rm xc}[n_0(z)] \ , \tag{2.6}$$

where $n_0(z)$ is the bare surface electron density.[38] Following Ref. 38 we use the corrected form of Wigner's expression[39] for the exchange-correlation energy $\mu_{\rm xc}$,

$$\begin{aligned}\mu_{\rm xc}(n)&=\frac{d}{dn}[n\varepsilon_{\rm xc}(n)] \ ,\\ \varepsilon_{\rm xc}(n)&=-\frac{0.458}{r_s}-\frac{0.44}{r_s+7.8} \ ,\\ \tfrac{4}{3}\pi r_s^3&=\frac{1}{n} \ ,\end{aligned} \tag{2.7}$$

where n is the local electron charge density. The potential $\Delta V^s(\rho,z;Z)$ calculated as outlined above for $r_s=2$ jellium, $\rho=0$, and $Z=10a_0$ is shown by the dotted curve of Fig. 1(b). The parameters Δ and z_0 that were used for σ in the calculation are listed in Table I. The vertical arrow in Fig. 1(b) indicates the magnitude of the reduction of $\Delta V^s(\rho,z;Z)$ resulting from the exchange-correlation correction, Eq. (2.5). It can be seen that this is a rather small correction to the surface potential.

Our procedure for calculating ΔV^s is approximate. Ideally one would like to calculate ΔV^s self-consistently. Even for a jellium model within the nonlocal DF approximation this represents a formidable task and to our knowledge has not been done. The ΔV^s term, however, varies rather slowly with z and has a relatively minor effect on the resonance energies. Our linear response approach is therefore adequate. In Sec. V we will further discuss the validity of this approximation and present some error estimates.

This completes presentation of our prescription for computing the quantities $V_0^s(z)$ and $\Delta V^s(\rho,z;Z)$ of Eq. (2.1). The complete one-electron potential thus requires only specification of the direct electron-ion potential, $V^A(\rho,z;Z)$. As discussed above, for the hydrogen atom $V^A(\rho,z;Z)$ is simply the Coulomb interaction $1/r=[(z-Z)^2+\rho^2]^{-1/2}$. For alkali atoms we approximate $V^A(\rho,z;Z)$ by pseudopotentials developed by Bardsley.[40] These angular momentum (l) dependent potentials have the form

$$V_\rho^l(r)=A_l r^p\exp(-\xi_l r^q)-\frac{\alpha_d}{2(r^2+d^2)^2}-\frac{\alpha_q}{2(r^2+d^2)^3}-\frac{1}{r} \ . \tag{2.8}$$

The parameters d, α_d, α_q, A_l, and ξ_l are listed in Table II.

B. Solution of the Schrödinger equation

An electronic state of an atom or molecule in the vicinity of a solid surface may have a finite lifetime with respect to resonant decay into a continuum of states of the solid, i.e., these states may be decaying resonance states rather than true bound states. Indeed, calculation of the lifetimes of such states is a primary objective of the present work. In the one-electron model employed here,

TABLE I. Parameters Δ and z_0 used in the evaluation of $\sigma(\rho,z,Z)$ [Eq. (2.4)].

	z_0 (a.u.)	Δ (a.u.)
$r_s=2$	0.85	1.74
$r_s=4$	0.45	2.25

TABLE II. Pseudopotential parameters (a.u.) for alkali-metal atoms as defined in Eq. (2.8) in the text.

	Li	Na	K	Rb	Cs
α_d	0.1925	0.945	5.47	8.966	15.0
α_q	0.112	5.0	41.5	102.0	230.0
d	0.75	1.1	1.5	1.95	2.0
$l_{\max}$	2	2	2	3	3
A_0	6.013 668	10.281 59	9.568 369	17.295 03	14.767 32
A_1	−0.740 679	2.692 467	2.897 295	2.851 747	2.960 707
A_2	−0.067 342	−1.452 763	−3.916 641	−1.553 162	−0.399 982
A_3				−1.380 882	−1.943 567
ξ_0	1.293 213	1.294 506	0.709 742	0.746 748	0.541 614
ξ_1	1.410 279	0.681 447	0.363 969	0.295 391	0.232 594
ξ_2	0.8	1.0	0.748 353	0.387 761	0.193 225
ξ_3				0.436 382	0.367 542

any atomic state with energy above the bottom of the jellium conduction band can decay by resonant tunneling into the conduction band, and is thus a resonance state. In order to obtain the energies and widths of the resonance states we employ a technique called complex scaling or "dilatation transformation."[41] This technique has been used extensively in atomic physics to calculate resonance lifetimes both for free atoms and for atoms in external fields. The advantage of this method is that resonance states, which are formally scattering or continuum states, can be computed using bound-state techniques, i.e., using a set of square integrable basis functions.

A simplistic description of the wave function Ψ of a resonance state is

$$\Psi(t)=\exp(-iEt/\hbar)\Psi(t=0) , \tag{2.9}$$

where the eigenenergy E is complex:

$$E=E_R-i\Gamma . \tag{2.10}$$

E_R and Γ are the real and imaginary parts of the energy, respectively. Thus $\Psi(t)$ decays in time with a lifetime $(2\Gamma)^{-1}$. Our objective is to compute both the energy E_R and the width Γ as a function of the distance of the atom from the surface for the electronic states of interest. A Hermitian Hamiltonian, however, can produce only real eigenvalues for square-integrable eigenfunctions. The desired complex roots are associated with eigenstates exhibiting so-called Siegert (diverging) boundary conditions:

$$\Psi(r)\sim e^{ik_R\cdot r+k_I r}f(\Omega) \text{ as } r\to\infty . \tag{2.11}$$

Complex scaling is a procedure for transforming the original Hermitian Hamiltonian into a non-Hermitian Hamiltonian which exhibits square integrable eigenfunctions with complex eigenvalues.

The procedure, as we implement it here, is as follows: the coordinate $\mathbf{r}$ designating the position of the electron relative to that of the ion core is "rotated" into the complex plane by an angle θ, $0<\theta<\pi/2$:

$$\mathbf{r}\to\mathbf{r}e^{i\theta} . \tag{2.12}$$

The rotated Hamiltonian is obtained simply by everywhere substituting $\mathbf{r}e^{i\theta}$ for $\mathbf{r}$. $H(\theta)$ is then given by

$$H(\theta)\equiv H(\mathbf{r}e^{i\theta}) = e^{-2i\theta}\frac{\nabla^2}{2}+V(\mathbf{r}e^{i\theta}) . \tag{2.13}$$

Upon this rotation the resonance boundary conditions take the form

$$\Psi(r)\sim e^{i(k_R\cos\theta+k_I\sin\theta)r+(k_I\cos\theta-k_R\sin\theta)r}f(\Omega) \text{ as } r\to\infty . \tag{2.14}$$

For $\theta>\arctan(k_I/k_R)$, this is transformed into a bound-state boundary condition. Formal aspects of the complex-scaling approach have been examined in depth and it has been shown rigorously[42] that, for a class of potentials ("dilatation analytic") $V(\mathbf{r})$, this mathematical transformation has the following consequences. (1) The bound-state eigenvalues of $H(\theta)$ are identical to those of the original Hamiltonian H. (2) The scattering thresholds are unchanged by this transformation. (3) Complex eigenvalues of $H(\theta)$ may arise corresponding to square-integrable eigenfunctions. It is the latter that are associated with resonance states, with real and imaginary eigenenergies, E_R and $\Gamma/2$, with the same meaning as in Eq. (2.9). Thus by performing the complex rotation on the Hamiltonian, we can obtain both bound and resonance states via the same calculation using only square integrable basis functions. The advantage of simpler boundary conditions is at the expense of having to deal with a non-Hermitian complex Hamiltonian. This lengthens the computation time somewhat, but is not a serious problem.

In this application we solve the one-electron Schrödinger equation by expanding the wave function in a basis consisting of generalized Laguerre polynomials:

$$\phi_{nlm}=e^{-\lambda r/2}r^{l+1}L_n^{2l+2}(\lambda r)Y_{lm}(\Omega) , \tag{2.15}$$

where λ is a parameter that can be used to optimize the basis. For each angular momentum quantum number l, we include $n(l)$ radial functions. The basis set is thus specified by a vector $(n(0), n(l), \ldots, n(l_{\max}))$. Typical values of $l_{\max}$ employed were 15 and $n(l)$ ranges from 10 to 40.

The matrix elements of the complex Hamiltonian are easily evaluated and the Schrödinger equation is convert-

ed into a matrix equation which is solved by direct diagonalization. This task is computationally quite fast, even for the largest basis sets employed. The details of the procedure are elaborated in the Appendix.

If the basis set is large enough to be essentially complete, the method approaches the formally exact result. The resonance energies and widths will be independent of θ as long as θ is large enough to "expose" the resonance $[\theta > \arctan(k_I/k_R)]$. In practice, a limited basis must be used and both the real and imaginary part of the resonance energies will vary slightly with θ. The eigenvalues will, therefore, form trajectories in complex coordinate space. The θ dependence of the resonance eigenvalues introduces some uncertainty in the results, but also provides an estimate of the error introduced by the use of a limited basis. It has been shown that under certain conditions the complex energies satisfy a generalized variational principle,[43] such that, with a limited basis, the true resonance energy will be stationary with respect to θ. Using this criterion the resonance eigenvalues can be obtained directly from the stationary points of the eigenvalue trajectories. In Fig. 2 we give examples of complex energy trajectories for one of the hydrogen $n=2$ resonances for different choices of basis sets. Each figure contains ten dots representing θ varying from 0.15 to 0.6. For Figs. 2(a) and 2(b), we used a basis set containing 49 basis functions, $n=(7,7,7,7,7,7,7)$. For Fig. 2(a) $\lambda=0.66667$ was used. It can be seen that the real and imaginary parts of the resonance energy vary relatively strongly with θ. In Fig. 2(b) the value $\lambda=1.0$ was used. This choice of λ corresponds to the correct wave function for the $n=2$ states of a free hydrogen atom. It can be seen that the θ trajectory for this choice of basis is much more confined. In Fig. 2(c), a slightly larger basis set is used $n=(8,8,8,8,8,8,8,8)$ and $\lambda=0.66667$. This larger basis set reduces the θ variation considerably compared to Fig. 2(a).

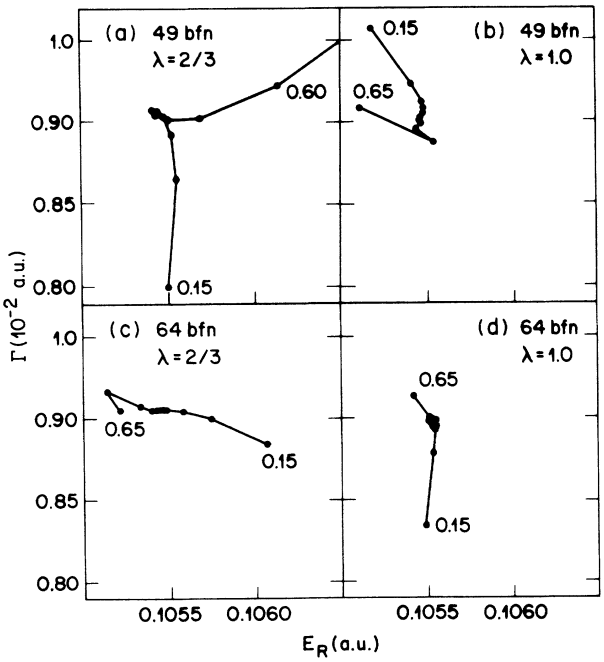

FIG. 2. Examples of trajectories of the resonance eigenvalues as functions of rotation angle θ. The calculation refers to one of the H ($n=2$) resonances for H/Al at $z=10$. (a) shows trajectories with a small basis set. In (b) we show trajectories for a larger basis set. (c) uses the same basis as in (a) but with $\lambda=1$. In (d) we show the trajectories using $\lambda=1$ and a large basis.

For Fig. 2(d) we used the larger basis set with the more appropriate $\lambda=1$. Here the θ trajectory is very compact, and the resonance energy can be obtained to three significant digits. Increasing the size of the basis further confirms the results from Fig. 2(d). Thus for this one-electron application the method is very efficient. Even with a modest set of 49 basis functions the resonance energy and lifetime can be obtained to two significant figures. Increasing the basis set and verifying convergence does, however, serve as a valuable check that the correct resonance eigenvalue has been obtained. The calculations described below were typically performed with 225 basis functions, and we are confident that the accuracy of the results is better than three significant figures.

III. RESULTS

In the following section, we present results of calculations of the energies and lifetimes of atomic electron states in the vicinity of jellium surfaces. In Sec. III A we discuss hydrogen on different surfaces. Hydrogen is the simplest of all adsorbates and it is a true one-electron atom. In Sec. III B we give results on alkali atoms on jellium. For the alkalis, we employ a pseudopotential to remove the core electrons and reduce the alkalis to approximate one-electron atoms as well.

A. Hydrogen

In a previous publication[31] we presented results for the level shifts and broadening for a hydrogen atom in the vicinity of $r_s=2$ (Al) and $r_s=4$ (Na) jellium surfaces. Here some additional results are presented. One of the characteristic features of a hydrogen atom interacting with a metal surface arises from the degeneracy of hydrogenic states. The surface potential lifts the degeneracy and causes the hydrogen states to hybridize and mix with each other. This is illustrated in Fig. 3, where we show how the real and imaginary part of the lowest hydrogen levels vary with distance from an Al ($r_s=2$) surface. The real parts of the hydrogen states show a somewhat complicated variation with distance. The hydrogen-surface interaction results in the formation of hybrid states similar to "Stark states."[44] These hybridized states form at large distances from the surface since an infinitesimal linear component of the surface potential is sufficient to lift the asymptotic degeneracy of the states. For the $n=2$ states, the symmetry of the surface allows the $2s$ state to interact with only the $2p_z$ state within the $n=2$ manifold. The Stark states $2s+2p_z$ and $2s-2p_z$ then form. In the upper part of Fig. 4 we show schematically what these states look like. The orbitals are oriented away from and towards the surface respectively. The $2p_x$ and $2p_y$ states do not mix.

At smaller atom-surface separations, the hybridization

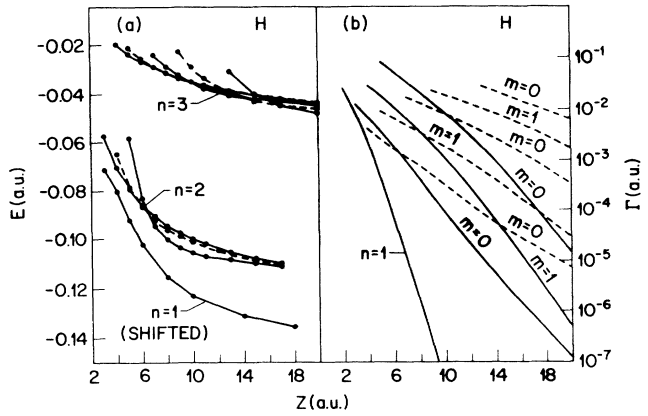

FIG. 3. Calculated energy shifts and widths for hydrogen on Al. In the left part of the figure, the real part of the energy is shown. The $n=1$ state has been shifted 0.35 a.u. upward in energy. The solid curves are the $m=0$ states. The dashed curves are the $m=1$ states. Distances are in a.u. measured from the jellium edge and energies in Hartrees.

of the states becomes more complicated, and additional mixings with surface electronic states occur. There are several level crossings, as shown in Fig. 3. A rough understanding of why the crossings occur can be obtained from the following arguments: The full electron-surface interaction is attractive at large distances from the surface and repulsive at short distances. The electron densities of the $2s-2p_z$ and $2s+2p_z$ hybrids are shifted toward and away from the surface, respectively, and the $2p_{x,y}$ state is centered on the proton. Thus, as the atom approaches the surface from a large distance, the $2s-2p_z$

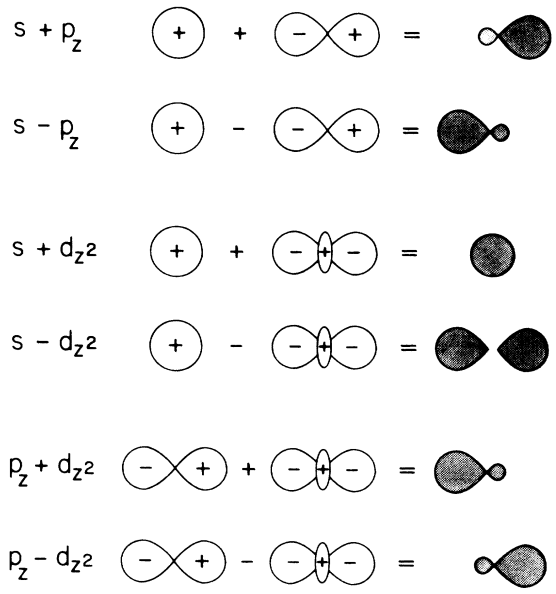

FIG. 4. Schematic illustration of the surface hybridized states. The $2s$ and $2p_z$ states hybridize and form $2s+2p_z$ and $2s-2p_z$ states. We also show a schematic representation of the states resulting from *s-d* and *d-p* hybridization.

is most attractive. At shorter distances this same state exhibits the strongest repulsion due to overlap with the surface electron cloud. Thus crossings must occur as shown in Fig. 3. We note that for the complex non-Hermitian Hamiltonian that results from the complex-scaling procedure, the "noncrossing" rule does not apply. Not only can the real parts of the energies of states of different symmetry be equal, but so can those of the same symmetry. Thus the real parts of the energies can exhibit actual crossings or avoided crossings, and we observe both in the examples below. Since it is difficult to determine whether numerical curves actually cross or are avoided by a tiny amount, we will simply refer to crossings as all cases for which the curves approach to within the precision of the calculation, about 10^{-4} a.u.

While there are relatively small differences in the real parts of the energies of the different hybridized states, their corresponding lifetimes are extremely different. This is because the widths are determined by electron tunneling between the hydrogen and the surface. Since tunneling rates are exponential functions of the distance, there will be a large difference in the tunneling rate depending on whether the orbital is oriented towards the surface, parallel, or away from the surface. Figure 3 shows, as expected, that the state pointing towards the surface has the largest width and the state oriented away from the surface is most narrow.

The $n=3$ levels are also plotted in Fig. 3. The $n=3$ state is asymptotically ninefold degenerate. The surface potential lifts the degeneracy, producing six distinct states (three nondegenerate $m=0$ states, two doubly degenerate $m=1$, and one doubly degenerate $m=2$). Curve crossings are exhibited by these states as well. The lifetimes of the various hybridized orbitals differ even more than for $n=2$. This is due to the increasing possibilities of hybridization when an extra state is added. The most longlived of the $n=3$ states has almost as long a lifetime as the most longlived of the $n=2$ states in the depicted region.

B. Alkali atoms

We now present results of calculations for the alkali atoms (Li,Na,K,Rb,Cs) near $r_s=2$ and $r_s=4$ jellium surfaces. The only change from the H atom calculations described above is the replacement of the $-1/r$ Coulomb potential by pseudopotentials as discussed earlier. One-electron calculations using these pseudopotentials reproduce the energies of the ground state and the lowest few excited states for the atoms in vacuum with very high accuracy. Furthermore, they have been successful in calculations of the binding of alkali dimers, suggesting that not only the energies but also the resulting wave functions are quite accurate.[40] The pseudopotential depends on angular momentum, l, and the matrix elements are evaluated using complex basis functions as outlined in the Appendix.

In Figs. 5–9 we present calculations of the energies and the shifts of the ground and lowest excited alkali atom states in the vicinity of a $r_s=2$ jellium surface, i.e., aluminum. We will discuss each figure separately but we

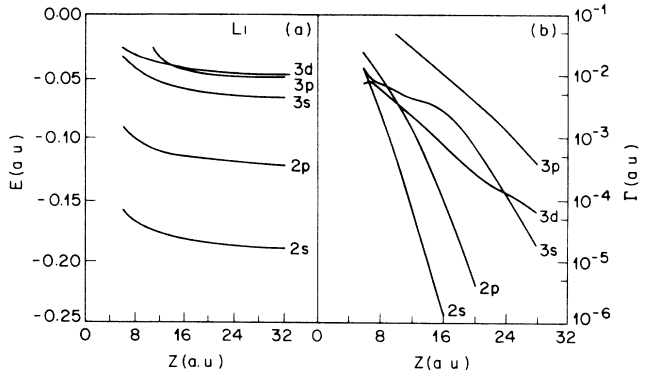

FIG. 5. Calculated energy shifts and widths as a function of atom surface separation for the $m=0$ states of Li/Al. Distances are in a.u. measured from the jellium edge and energies in hartrees. States are labeled by their asymptotic limits.

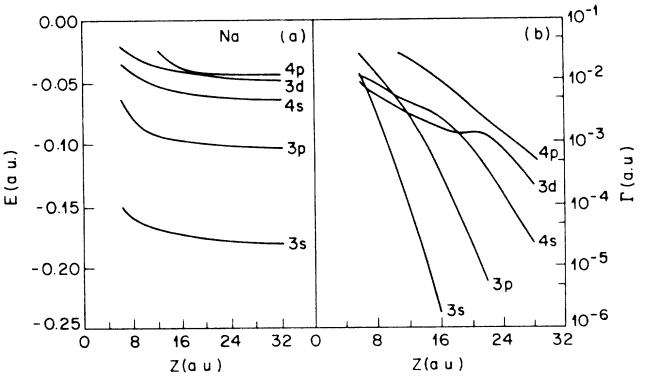

FIG. 6. Calculated energy shifts and widths as a function of atom surface separation for the $m=0$ states of Na/Al. The units and notations are the same as in Fig. 5.

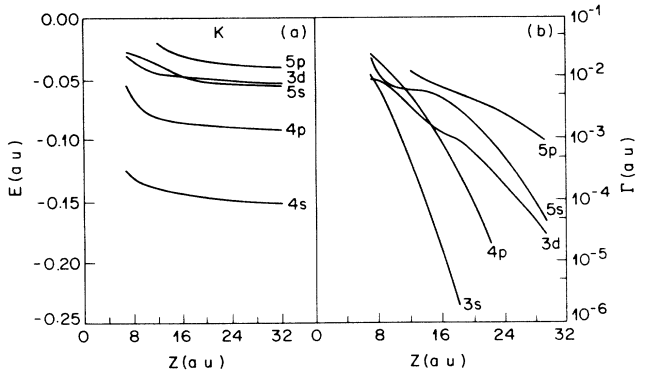

FIG. 7. Calculated energy shifts and widths as a function of atom surface separation for the $m=0$ states of K/Al. The units and notations are the same as in Fig. 5.

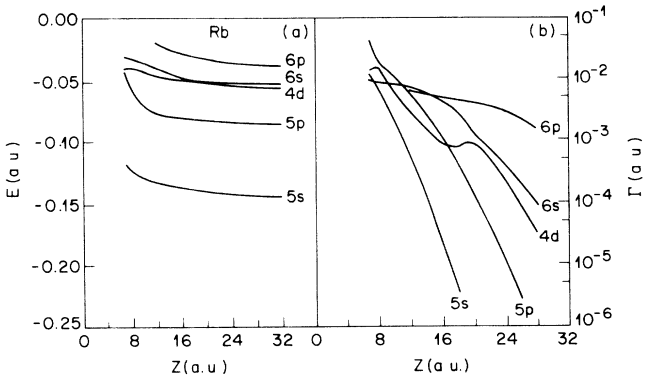

FIG. 8. Calculated energy shifts and widths as a function of atom surface separation for the $m=0$ states of Rb/Al. The units and notations are the same as in Fig. 5.

will start with some general comments. The application to alkali atoms shows some distinct new features compared to hydrogen. A fundamental difference is that in the alkalis the different angular momentum states for the same principal quantum number, n, are asymptotically nondegenerate. The hybridization of the atomic levels with the surface is, therefore, normally much less extensive than in the case of hydrogen. The excited levels of the alkalis are, however, relatively closely spaced in energy. Due to the differences in spatial extent of the atomic orbitals, the energies can shift differently. Because of these facts, there are several possibilities for curve crossings and avoided crossings. In the vicinity of these crossing points, atomic states of the correct symmetry can hybridize strongly. In the case of s- and p-level crossings, the resulting states will be similar to the Stark states. We also encounter s-d and p-d hybridization. This also leads to orbitals that are oriented away from or towards the surface. In Fig. 4, we show a schematic plot of some of the different hybrid orbitals that are encountered. As was the case in the hydrogen problem, the lifetimes of such surface hybridized states can be drastically different from each other and from those of the parent unhybridized states.

The surface potential is a rather complicated function

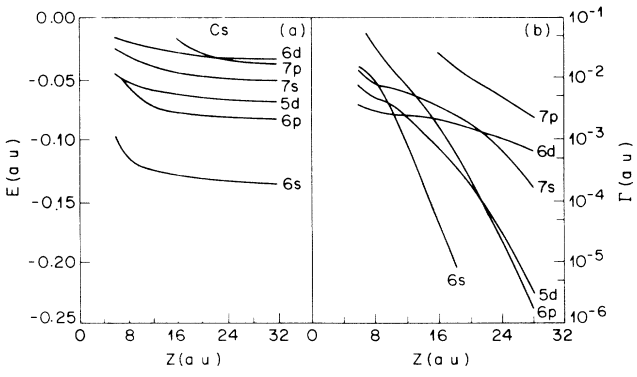

FIG. 9. Calculated energy shifts and widths as a function of atom surface separation for the $m=0$ states of Cs/Al. The units and notations are the same as in Fig. 5.

of the electron and ion core coordinates. The shifts and broadening of the atomic levels reflect the complexity of the potential and it is difficult to give a detailed account of how the resonances behave as function of atom-surface separation. It is appropriate, however, to state some general observations.

All states eventually shift upwards to higher energy (lower ionization potential) with smaller atom-surface separation. The magnitudes of the shifts are different for the different states and basically are determined by two effects. The spatial extent of the orbital determines how rapid the upshift will be. A large orbital averages the surface potential over a large region and, therefore, shifts more smoothly with distance than a compact orbital which basically will follow the image potential. The same trend also applies to the variation of the widths with distance. The other factor that influences how the resonances vary with distance is the orientation of the atomic state. The energies of the states for which the electron density is shifted towards the surface will vary faster with distance than states that are oriented parallel to or away from the surface. This is because it is the electron-core image repulsion that is primarily responsible for the upshift of the electronic states. The potential is largest in the direction towards the image core, i.e., towards the surface. The states that are oriented towards the surface also have larger widths than states that lie along or away from the surface. As we discuss Figs. 5–9 separately, we will see that the energy shifts of the alkali levels are relatively smooth functions of distance. The widths, on the other hand, show a much more complicated behavior, due primarily to changing degrees of hybridization.

In Fig. 5 we show the lowest energy $m=0$ states of Li. The $3p_z$ and $3d_{z^2}$ states are asymptotically very close in energy and are fully hybridized in the depicted region ($Z<32$ a.u.). The p and d hybridization results in two states, schematically depicted in Fig. 4. One state $p+d$ is oriented towards the surface and the other, $p-d$ points in the vacuum direction. The state oriented towards the surface and has a shorter lifetime and crosses the $p-d$ state since it shifts faster with distance.

In Fig. 6 we show the variation with distance of the lowest Na levels ($m=0$). The $3d_{z^2}$ and $4p_z$ levels are well separated at the largest distance. The $3d$ state shifts slightly faster than the $4p$ level and at a distance of around 15 a.u., the states start to hybridize analogous to the $3p$ and $3d$ levels of Li. The energies of the two states are clearly separated. The hybridization has a dramatic effect on the resonance widths as a function of distance, producing a distinctly nonexponential decay of width with distance from the surface. The p-d hybridization produces states that have their weights shifted towards or away from the surface. The state correlating asymptotically with $3d$ forms the hybrid that is shifted towards the vacuum. The width of this state is dramatically reduced since the part of the $3d$ function oriented toward the surface is largely cancelled. The state correlating with $4p$ becomes the hybrid that is oriented toward the surface. The width of this state increases more rapidly in the vicinity of the curve crossing since the surface oriented part of the state gets more weight.

In Fig. 7 we show the lowest $m=0$ states for K. The $3d_{z^2}$ and $5s$ states are initially relatively far apart and the states are not hybridized. As the atom approaches the surface, the $5s$ state shifts more than the $3d$ and the states approach each other. At $Z=17$ a.u. there appears to be a crossing. The hybridization is relatively weak and results in an extended state, $s+d$, and a compact state $s-d$, as illustrated schematically in Fig. 4. Again, the hybridization has a large effect on the lifetimes of the levels. This effect can be seen most clearly by considering the slopes of the curves of the level widths as a function of distance. After the hybridization the width of the $3d$ state increases much more slowly with decreasing distance than before the interaction. The width of the $5s$ increases faster with decreasing distance.

In Fig. 8 we show the lowest $m=0$ states for Rb. The $6s$ and $4d_{z^2}$ levels do not significantly hybridize at large distances. The $4d$ level shifts faster with distance than the $6s$ level and at 18 a.u. the states come relatively close to each other and start to interact. The s-d hybridization results in an extended state with relatively short lifetime and a compact state with longer lifetime. For Rb the hybridization is very large and the state that is derived from the $4d$ actually reduces its width as the surface is approached. The $6s$ state increases its width more strongly than in the absence of the interaction. The energy levels do not cross each other but follow each other closely.

In Fig. 9 we show the variation with distance of the energies of Cs $m=0$ states. The $7p_z$ state shifts faster than the $6d_{z^2}$ state, and at $Z=22$ a.u., the states come close to each other. The hybridization is weak and there appears to be a crossing of the levels. The widths of the states change slightly as a result of the hybridization. At $Z=8$ the $5d_{z^2}$ and the $6p_z$ levels come close to each other. The hybridization is rather weak but can clearly be detected from the change of slope of the widths as a function of separation from the surface.

IV. THE ROLE OF THE SURFACE POTENTIAL

In this section we investigate in some detail how the widths of the atomic resonances are influenced by the surface potential. We start by noting that the real and the imaginary parts of the resonance energies are sensitive to different parts of the surface potential. From perturbation theory it is known that the shift of an atomic level depends primarily on the overlap between the atomic state and the potential, i.e., the shift depends mainly on the potential in the region where the electron density is large. The width, on the other hand, is determined by tunneling of an electron between the atom and the surface. The WKB expression for the tunneling current between two points involves an integral of the potential over the region between the points. The width of the resonance is thus sensitive to the variation of the surface potential in the entire region between the adsorbate and the surface. The use of different prescriptions for obtaining the potential is the primary source of discrepancy between the present work and previous calculations.

We now illustrate these points with some examples. In Fig. 10 the widths of the Li $2s$ state as a function of dis-

tance on two different substrates, Al and Na, are plotted. It can be seen that the lifetime of the Li 2s level is shorter on Al. This can be understood directly from the difference in the surface potential between these substrates. For the argument it suffices to consider only the bare surface potential. There are also some differences in the repulsive electron-core image potential, since the location of the image plane and the width of the induced charge distribution, Δ, are different on Al and on Na. Since the variation of $\Delta V^s(\rho,z,Z)$ with z is relatively smooth, these differences are relatively minor. In the lower part of Fig. 10 the bare surface potential $V_0^s(z)$ is plotted for Na and Al. Na is a low-electron density substrate with a rather extended surface potential. The surface potential $V_0^s(z)$ for Al varies much faster and is more confined to the surface. From the WKB approximation it is clear that the widths of the atomic resonances depend strongly on the breadth of the potential barrier between the adsorbate state and the surface. These breadths $l_{\rm Al}$ and $l_{\rm Na}$ between the Li and the two different metals are also indicated in the figure. As can be seen in Fig. 10, due to the fact that the surface potential varies more gradually for Na, the breadth of the barrier $l_{\rm Na}$ is larger. Thus the width of the Li 2s level is smaller for Na than for Al.

In Fig. 11 we show the shifts of the lowest hydrogen

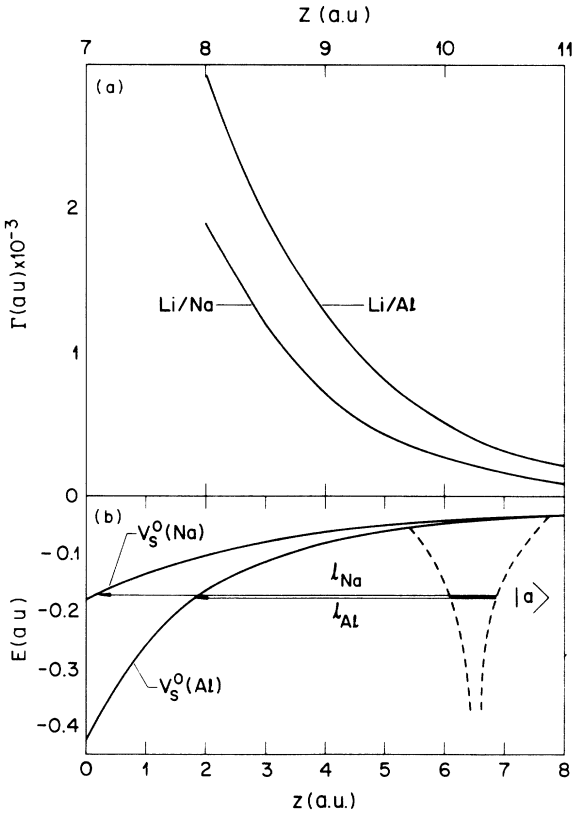

FIG. 10. (a) Calculated width of the Li 2s resonance as a function of distance from an Al and a Na substrate. (b) The bare surface potential $V_0^s(Z)$ for an Al and a Na substrate. The atomic potential is schematically indicated with a dashed line. The energy of the Li 2s state is also indicated. All units are in a.u.

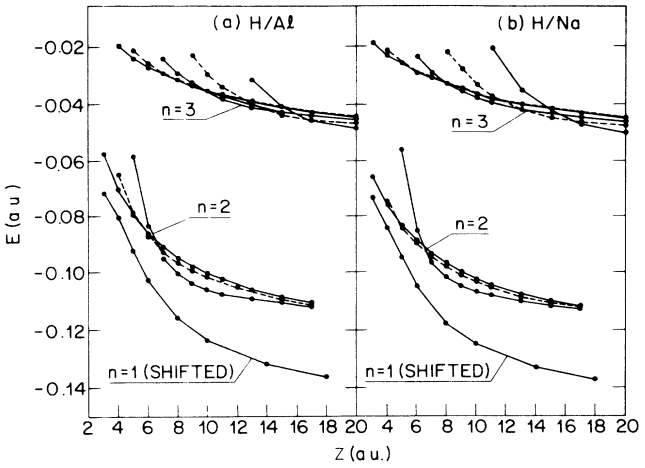

FIG. 11. Variation of the real part of the lowest excited H levels with distance from the jellium edge. (a) is for H on $r_s=2$ jellium (Al) and (b) is for H on $r_s=4$ jellium (Na). The units and notations are as in Fig. 4.

states as a function of distance outside an Al and a Na surface. From the figure it can be seen that the energy shifts are very similar. This is due to the fact that at $Z>5$ a.u. the potential outside Al and Na is fairly similar (see Fig. 10), and basically determined by the image interactions. Since the shifts of atomic levels depend mainly on the potential in the region of overlap with the atomic wave function, both metals will induce roughly the same shift. Also in this situation the width of the H resonances will be much larger for H/Al than H/Na. This fact is most clearly seen by considering the $n=1$ state. H ($n=1$)/Na has zero width while for Al this resonance can be very broad (see Fig. 3).

The result that electronic levels of atoms at physisorption distances are broader on Al than on Na is not obvious and in direct contradiction to what has been found using approximate methods.[30] Al has a higher work function than Na so the electron distribution is more confined to the surface for Al. One might, therefore, have expected lower tunneling rates outside Al surfaces. Tunneling is, however, a resonant process and to describe the process one must take into account both the spatial and energy distributions of the states. The golden-rule expression for the broadening of a discrete level $|a\rangle$ interacting with a continuum of states $|\mathbf{k}\rangle$ is

$$\Gamma=\pi\sum_{\mathbf{k}}|V_{a\mathbf{k}}|^2\delta(\varepsilon-\varepsilon_{\mathbf{k}})\ . \tag{4.1}$$

$V_{a\mathbf{k}}$ is the perturbation matrix element between the level $|a\rangle$ and the states $|\mathbf{k}\rangle$. At any given energy ε there are in general more states $\mathbf{k}$ with $\varepsilon_{\mathbf{k}}=\varepsilon$ in a large bandwidth metal such as Al than on Na. Thus, since this dominates the difference between the $V_{a\mathbf{k}}$'s, Γ will be larger on Al than on Na.

A straightforward application of the golden rule to the calculation of atomic-level broadening is, however, not possible, except at very large separations from the surface. When the adsorbate state is introduced, the metal states must orthogonalize to the atomic wave function.

This orthogonalization perturbs the metal states significantly[45] and the unperturbed metal states are unsuitable for a perturbation expansion of the bare adsorbate-metal potential. The present approach of solving the Schrödinger equation includes these effects and preserves the orthogonality of the atomic and the surface (nonresonant scattering) electronic states.

An important consequence of the fact that extended surface potentials will give rise to smaller broadening of physisorbed atoms is that calculations using LDA will overestimate the widths of atomic resonances. As was depicted in Fig. 1, the LDA surface potential rises more steeply towards the vacuum than the DF potentials which include the image forces. In Fig. 12 we compare the widths of the H ($n=2$) resonances on an Al surface modeled using z_0 and $V_0^s(z)$ calculated in the present nonlocal approximation (solid line) and in the LDA (Ref. 21) (dotted line). It can be seen that calculations using the LDA description overestimate the widths of the atomic states. At a distance of 7 a.u. the $2s+2p_z$ state which is oriented towards the vacuum is 50% broader using LDA than with the DF description of the surface potential. The $2s-2p_z$ states that are oriented towards the surface differ by less than 10%. This is because LDA gives a good description of the surface potential close to the selvedge.

As was mentioned in Sec. II A, the total surface potential for the ionization level of a H atom contains two parts, an attractive electron-electron image interaction and a repulsive electron-core image interaction. In calculations based on a mean field approximation such as the local-density approximation,[46,47] one does not distinguish between the different contributions to image charges but considers only the electrostatic interaction between the atom and the surface. In the case of a neutral adsorbate the electron-core image interaction is not included and there is no repulsive barrier between the adsorbate and the surface. This leads to too large a width for the atomic levels. The dashed curves in Fig. 12 are the widths of the H ($n=2$) states calculated using LDA with neglect of the electron-core image repulsion. LDA in the mean field approximation can thus overestimate level widths for neutral atoms far from the surface by up to a factor 4. With decreasing atom-surface separation the atomic wave function starts to overlap with the surface wave functions. Close to the surface the electron-core image repulsion will be included and the level widths thus calculated properly. These facts show that the variation of neutral atomic level widths with distance will be underestimated using the LDA. These arguments could be a possible explanation for the finding by Lang *et al.*[8] that the widths of the ionization levels of noble gas atoms physisorbed on metals seems to be only weakly dependent on atom-surface separation.

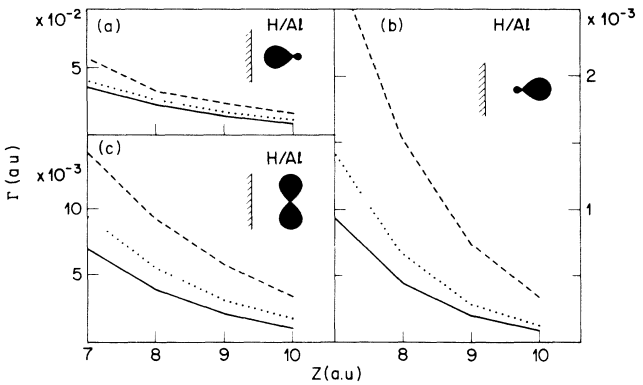

FIG. 12. A comparison of the widths for the three H ($n=2$) resonances as a function of distance outside an Al surface using different many-body descriptions. The solid lines are the results using DF theory. The dashed lines are the results obtained using LDA theory and the mean-field approximation. The dotted lines are the results obtained using the LDA but including the electron-core image repulsion. To distinguish between the different H ($n=2$) states their orientation is schematically indicated on each figure. All units are in a.u.

V. DISCUSSION

There is mounting experimental evidence[48–51] that calculated excited state lifetimes reported previously are too short. Our present demonstration of much longer lifetimes for electronic states at surfaces means that resonance tunneling charge transfer must occur somewhat closer to the surface than previously believed. It also means that there will be much more "memory" of the initial configuration in the final state of a particle emerging from a surface than what has been assumed. For instance, in scattering experiments, the final state can be more strongly affected by processes that occur at the impact of the particles with the surface. In the region close to the surface the adsorbate levels can be strongly affected by various physical effects such as adsorbate-substrate hybridization and promotion, and estimates of level shifts based only on the image potential will not be accurate.

In a recent experiment[51] the neutralization rate of alkali ions scattered from a cesiated tungsten surface was studied. It was shown that the conventional theories for charge exchange in atom-surface reactions using previously published (short) lifetimes[30] fail to explain the data. The consequence of short lifetimes for such a process is that as soon as the work function becomes smaller than the ionization energy, neutralization can occur with high probability. This leads to an approximately steplike behavior in the neutralization efficiency as a function of work function. The experiment revealed a relatively smooth variation of the neutralization efficiency with work function. In a recent publication[52] it is shown that the data of the experiment is in accord with the longer lifetimes calculated in the present paper, provided that the effects of memory and local fields are included.

In a recent sputtering experiment on metal surfaces the velocity distribution of excited metal atoms was determined.[53] The experimental results show that excited metal atoms with low velocities can be detected. This finding again indicates that the lifetimes of the excitations are relatively long on the surface. Resonant deexcitation of a sputtered atom seems to occur only very close to the surface where the atomic level hybridizes strongly with the substrate levels. This is again in agreement with our

finding of long lifetimes of excited atomic states.

In electron stimulated desorption from metal surfaces[54] significant fractions of excited H have been observed. The excited H are assumed to be formed at some distance z_0 from the surface. As the H recedes from the surface the excited states can decay. Interpretations[30] using the previously calculated short lifetimes for the hydrogen $n=3$ state have been forced to assume that the H ($n=3$) is formed at very large distances from the surface, $z_0 \approx 20$ a.u. It is difficult to conceive of a mechanism for creating excited H at this large distance. An interpretation using the present longer lifetimes give the more reasonable $z_0=5$ a.u. In addition, in recent electron stimulated desorption experiments from alkali covered metal surfaces,[55] a linear dependence of the excited H fraction on alkali coverage has been observed. As we have discussed above for alkalis, such a finding is inconsistent with the earlier proposed short lifetimes which predict a sharp steplike decrease of the yield of excited H with work function. The results are consistent with the present finding of long lifetimes.[52]

In principle, one can obtain an upper bound to the lifetime-induced width from experimental spectra. However, the direct comparison of calculated excited electronic state lifetimes with experimentally determined widths is complicated by the many contributing factors to experimental line broadening. In addition, the equilibrium bond lengths of physisorbed species are generally not known accurately.

In recent NMR experiments[56] it was concluded that the width for the Li $2s$ state on Fe is 1.0 eV. Assuming a Li metal bond length of 2.5 a.u. (corresponding to the calculated equilibrium distance of Li on $r_s=2$ jellium) and modeling the surface with jellium of $r_s=2$ our calculated width is 1.2 eV. This is in relatively good agreement with the NMR experiments.

Spectroscopic studies of the electronic structure of physisorbed alkali atoms is complicated by various types of collective as well as final-state effects[57] and have, to our knowledge, not yet been able to provide unambiguous estimates for widths and shifts of alkali levels. The experimental situation is better for inert gases physisorbed on metals. It has been pointed out by Lang *et al.*,[8] that the lifetimes of excited noble gases should be very similar to the lifetimes of the ionization levels of the corresponding alkali atoms at the same distance from the surface. Thus the width of the excitation of a physisorbed inert gas can provide information about the lifetime of alkali atoms on metal surfaces. In Ref. 49, Xe physisorbed on Al was studied. The width of the Xe $7s$ level was found to be 0.2 eV. A self-consistent field (SCF) LDA calculation for Cs adsorbed at an assumed distance of 5 a.u. gives a width of 1–1.5 eV. A SCF LDA calculation for Cs adsorbed on Al using the present scheme gives a width of 1.4 eV while our proposed DF method gives a width of 1.1 eV. The difference between LDA and DF approximations is thus too small to account for the large difference between the calculated Cs ionization level widths and the experimentally measured width of the adsorption spectra for Xe. Possible reasons for this difference could be the assumption of an incorrect equilibrium distance for the atoms (for a bond length of 9 a.u., the calculated width is 0.2 eV) or excitonic effects (i.e., interactions between the $6p$ hole and the $7s$ electron) in the excited noble-gas atom. We cannot, however, exclude the possibility that density-functional theory is inadequate for the calculation of widths at short distances from metals.

The principal source of error in the present calculation comes from our approximate treatment of the surface potential. Ideally the surface potential should be calculated self-consistently. Unfortunately, a self-consistent calculation of the electron potential in a physisorption system using nonlocal-density-functional theory at present appears intractable. Thus in the present work a linear response approach has been used to construct the surface potential. Such an approach is not valid close to the surface. In order to test the quality of this approximation at distances close to the surface, we have performed a series of calculations using the LDA surface potentials (Sec. IV) for alkali atoms chemisorbed on Al ($r_s=2$) surfaces. The bond distances for this test are short and the results can be directly compared with fully self-consistent LDA calculations for the same systems. The results are summarized in Table III. It can be seen that even for quite small distances from the surface the calculated resonance widths are within 50% of those obtained using the SCF method. We therefore conclude that the present linear response approach for calculating ΔV^s is adequate for $z \gtrsim 5$ a.u.

Another approximation we have employed in the construction of the surface potential is the use of the LDA parameters when calculating the image charge distribution σ [Eq. (2.4)]. In order to test this approximation, a series of calculations were made for the width of the $2p_{x,y}$ states of H at $Z=10$ a.u. outside Al, for different parameters z_0 and Δ. The results are summarized in Table IV. It can be seen that the calculated widths are very insensitive to the magnitudes of these parameters. The reason, as was mentioned in Sec. II, is that ΔV^s varies only weakly with z and therefore, does not strongly influence the widths.[58,59]

Another source of error is the use of pseudopotentials for the alkali atom cores. The magnitude of the hybridization between the valence levels of the alkali atoms depends on the details of the wave functions of the involved atomic states. The pseudopotential does not reproduce the wave functions exactly. The calculated resonance energies for the alkali atoms are, therefore, approximate. The exact location of the crossing points are, of course,

TABLE III. Comparison of widths calculated using the present approach and the local-density approximation (Sec. IV) with those obtained using SCF methods. The substrate is Al (jellium $r_s=2$).

Level	Z (a.u.)	FWHM (eV) Present	SCF
Na $3s$	3.0	2.0	1.9[56]
K $4s$	4.0	1.6	1.4[57]
Cs $6s$	4.57	1.4	1–1.5[51]

TABLE IV. Calculated widths of the $2p_{x,y}$ states of H at $Z=10$ a.u. outside Al for some different parameters z_0 and Δ.

z_0 (a.u.)	Δ (a.u.)	$\Gamma/2$ (a.u.)
0.85	1.74	1.15×10^{-3}
−0.15	1.74	1.15×10^{-3}
1.85	1.74	1.07×10^{-3}
0.85	0.87	1.18×10^{-3}
0.85	2.61	1.15×10^{-3}

also subject to some uncertainty. The qualitative aspects of the interaction such as the structure of the level width as a function of distance in the vicinity of crossing points are likely to be valid.

Finally, we note that the use of a one-electron description almost certainly breaks down close to the surface where the overlap between the atom and the surface wave functions is large. In this region two-electron processes such as Auger decay will be strongly competing and perhaps dominant. An attempt to estimate the relative importance of one- and two-electron processes as a function of atom surface separation will be made in the future.

VI. CONCLUSIONS

We have demonstrated that the complex-scaling technique can be used to calculate lifetimes of adsorbate resonances at surfaces. We have shown that previous calculations of excited state lifetimes are typically too large by several orders of magnitude. Our finding of long lifetimes may mean that the so called "memory term" must be taken into account in dynamical descriptions of atom-surface reactions. We have shown that the shifts of excited levels are not simply given by the image potential. Different excited states shifts differently depending on their extent and spatial orientation. We have also shown that the lifetimes of excited alkali states are not always simple exponential functions of distance from the surface. In situations where levels cross each other, the lifetime of an atomic state may even increase with decreasing distance. This means that some of the conventional theories for charge exchange in atom surface scattering must be modified since they are based on the assumption that levels decay exponentially. We find that the magnitude of the widths depend on the substrate. The lifetimes of alkali levels are longer on metals with low-electron density such as Na than on high-electron density substrates such as Al. We have shown that it is important to include the image force when calculating adsorbate level widths. The method we have employed and further extensions of it should have applications for a large number of important dynamical processes such as the lifetimes of image states, lifetimes of chemisorption systems, tunneling rates in quantum wells, scanning tunneling microscopy, and defect or impurity levels in solids. In atomic physics the method has successfully been applied to the Stark effect for two-electron atoms. We see no problem, in principle, in extending its applicability to treat negative ion level widths and auger rates for atoms adsorbed on surfaces.

ACKNOWLEDGMENTS

The authors acknowledge valuable discussions with P. D. Johnson, N. D. Lang, and N. H. Tolk. This work was supported in part by U.S. Air Force Office of Scientific Research University Research Initiative Contract No. F49620-86-C-0125DEF; by the U.S. Office of Naval Research under Contract No. N00014-86-K-0735; and by the U.S. Air Force Office of Scientific Research under Contract No. AFOSR-86-0150.

APPENDIX

In this appendix we outline the theoretical details involved in the calculation. The starting point in the calculation is the one-electron Schrödinger equation:

$$[-\tfrac{1}{2}\nabla^2+V^{\rm eff}(\rho,z;Z)]\Psi=\varepsilon\Psi\ , \tag{A1}$$

with $V^{\rm eff}$ given by Eq. (2.1). In the following we omit the variable Z denoting the nuclear coordinate. In spherical coordinates the Hamiltonian takes the form

$$H=-\tfrac{1}{2}\nabla^2+V^A(r)+V_0^s(r,\Omega)+\Delta V^s(r,\Omega)\ , \tag{A2}$$

where we have separated the coordinate dependence of the surface potential into a radial and angular part Ω. We introduce the complex rotation in the radial coordinate and the Hamiltonian takes the form

$$H(\theta)=-\tfrac{1}{2}e^{-2i\theta}\nabla^2+V^A(re^{i\theta})+V_0^s(re^{i\theta},\Omega)+\Delta V^s(re^{i\theta},\Omega)\ . \tag{A3}$$

We now solve this Hamiltonian with a basis set of generalized Laguerre polynomials,

$$\chi_{n,l,m}(r,\alpha,\phi)=C_{n,l}(\lambda)r^{l+1}e^{-\lambda/2r}L_n^{2l+2}(\lambda r)Y_{lm}(\alpha,\phi)\ . \tag{A4}$$

The matrix element of the kinetic energy factorizes

$$T_{n,l,m;n',l',m'}(\theta)=e^{-i2\theta}\int_0^\infty dr\int_0^\pi d\alpha\sin\alpha\int_0^{2\pi}d\phi\,\chi^*_{n,l,m}(r,\Omega)(-\tfrac{1}{2}\nabla^2)\chi_{n',l',m'}(r,\Omega)\ . \tag{A5}$$

Using the above expression for the basis function the two angular integrations can be performed analytically and the matrix element reduces to

$$T_{n,l,m;n',l',m'}(\theta)=-\frac{e^{-2i\theta}}{2}C_{n,l}(\lambda)C_{n',l'}(\lambda)\times\delta_{l,l'}\delta_{m,m'}\int_0^\infty dr\,r^{l+1}e^{-\lambda r/2}L_n^{2l+2}(\lambda r)\left[\frac{d^2}{dr^2}+\frac{l(l+1)}{r^2}\right]r^{l'+1}e^{-\lambda r/2}L_n^{2l'+2}(\lambda r)\ . \tag{A6}$$

For the hydrogen atom, $V^A(r)$ is just the Coulomb attraction $-1/r$. The matrix element of the Coulomb term has the form

$$C_{n,l,m;n',l',m'}(\theta)=-e^{-\imath\theta}\int_0^\infty dr\int_0^\pi d\alpha\sin\alpha\int_0^{2\pi}d\phi\,\phi^*_{n,l,m}(r,\Omega)\left[-\frac{1}{r}\right]\phi_{n',l',m'}(r,\Omega) \tag{A7}$$

and analogously with the kinetic energy term it can be reduced to a simple one-dimensional integral

$$C_{n,l,m;n',l',m'}(\theta)=-e^{-i\theta}C_{n,l}(\lambda)C_{n',l'}(\lambda)\delta_{l,l'}\delta_{m,m'}\int_0^\infty dr\,e^{-\lambda r}r^{2l+1}L_n^{2l+2}(\lambda r)L_n^{2l'+2}(\lambda r)\ . \tag{A8}$$

Thus the kinetic and Coulomb matrix elements are factorized into a real part that depends only on the basis set and a complex part that depends on the rotation angle θ. This means that these matrix elements can be evaluated using real arithmetic, $\theta=0$, and can then trivially be obtained for any complex angle θ. This is not true for matrix elements involving the surface potential. A considerable amount of computational effort is required for the evaluation of this matrix element. The matrix element has the form

$$V_{n,l,m;n',l',m'}(\theta)=\int_0^\infty dr\int_0^\pi d\alpha\sin\alpha\int_0^{2\pi}d\phi\,\chi^*_{n,l,m}(\rho,\Omega)\left[V_0^s(re^{\imath\theta},\Omega)+\Delta V^s(re^{\imath\theta},\Omega)\right]\chi_{n',l',m'}(r,\Omega)\ . \tag{A9}$$

For the present calculations, the surface potential is prescribed numerically and its analytic continuation is not known. If we perform a variable substitution $x=re^{i\theta}$, and integrate with respect to ϕ, the expression for V takes the form

$$V_{n,l,m;n',l',m'}(\theta)=e^{-i\theta}C_{n,l}(\lambda)C_{n',l'}(\lambda)\int_0^\infty dx\,e^{-\lambda xe^{\imath\theta}}(xe^{-\imath\theta})^{l+l'+2}L_n^{2l+2}(\lambda xe^{-\imath\theta})L_n^{2l'+2}(\lambda xe^{-\imath\theta})S_{l,m,l',m'}(x)\ . \tag{A10}$$

Here the basis functions are complex and the surface potential is real. The analytic continuation of the basis functions is trivial. We note that the radial part of the basis functions is not complex conjugated, since its imaginary parts came from a variable substitution; i.e., from complex rotation. The matrix S in Eq. (A10) is defined in the following way:

$$S_{l,m,l',m'}(x)=\int_0^\pi d\alpha\sin\alpha\,P_l^m(\cos\alpha)[V_0^s(x,\Omega)+\Delta V^s(x,\Omega)]P_l^{m'}(\cos\alpha)\delta_{m,m'}\ . \tag{A11}$$

This entity is real.

For the alkali atoms a pseudopotential [Eq. (2.8)] is used instead of the Coulomb potential. The corresponding matrix elements are evaluated using complex basis functions analogously to (A10). The expression takes the form

$$P_{n,l,m;n',l',m'}(\theta)=\delta_{ll'}\delta_{mm'}e^{-\imath\theta}C_{n,l}(\lambda)C_{n',l}(\lambda)\int_0^\infty dx\,e^{-\lambda xe^{-\imath\theta}}(xe^{-\imath\theta})^{l+l'+2}L_n^{2l+2}(\lambda xe^{-i\theta})L_n^{2l'+2}(\lambda xe^{-i\theta})V_p^l(x)\ , \tag{A12}$$

where V_p^l is the lth component of the pseudopotential defined in Eq. (2.8).

The integrals in the radial integrations of the matrix elements above all contain an exponential factor $e^{-\lambda r}$. The integrations can, therefore, very efficiently be performed using Gauss-Laguerre quadrature. The basis functions can be evaluated using the recursion relations for generalized Laguerre polynomials. A direct evaluation of the polynomials by means of Horners scheme does not provide sufficient accuracy for the higher-order polynomials (order larger than 30).

The eigenvalue problem is thus converted to a secular equation. Since all matrix elements are diagonal in the azimuthal quantum number m, different m states do not couple:

$$\det|H^m_{n,l,n',l'}(\theta)-\varepsilon(\theta)|=0\ .$$

The solution of this equation gives both the bound and the resonant states. Due to the fact that the basis set is limited, the eigenvalues will depend slightly on θ and perform a trajectory in complex-energy space (Sec. II B).

[1]D. Menzel and R. Gomer, J. Chem. Phys. **41**, 3311 (1964); P. E. Redhead, Can J. Phys. **42**, 886 (1964).
[2]P. J. Feibelman and M. L. Knotek, Phys. Rev. B **18**, 6531 (1978).
[3]D. Menzel, in *Desorption Induced by Electronic Transitions*, edited by R. H. Stulen and M. L. Knotek (Springer, New York, 1988), Vol. III.
[4]W. Ho, Comments Condens. Matter Phys. **13**, 293 (1988).
[5]M. L. Yu and N. D. Lang, Phys. Rev. Lett. **50**, 127 (1983).
[6]P. Nordlander and Ph. Avouris, J. Vac. Sci. Technol. A **5**, 698 (1987).
[7]J. E. Cunningham, D. K. Greenlaw, and C. P. Flynn, Phys. Rev. B **22**, 717 (1980).
[8]N. D. Lang, A. R. Williams, F. J. Himpsel, B. Reihl, and D. E. Eastman, Phys. Rev. B **26**, 1728 (1982).
[9]J. J. C. Geerlings, L. F. Tz Kwakman, and J. Los, Surf. Sci. **184**, 305 (1987).
[10]N. H. Tolk, J. C. Tully, J. S. Kraus, W. Heiland, and S. H. Neff, Phys. Rev. Lett. **41**, 643 (1978).
[11]B. Kasemo and L. Wallden, Surf. Sci. **53**, 393 (1975).
[12]R. Brako and D. M. Newns, Surf. Sci. **108**, 253 (1985).
[13]J. K. Norskov and B. I. Lundquist, Phys. Rev. B **19**, 5561 (1979).
[14]A. Blandin, A. Nourtier, and D. Hone, J. Phys. (Paris) **37**, 369 (1976).
[15]U. von Barth, in *Many-Body Phenomena and Surfaces*, edited

by D. Langreth and H. Suhl (Academic, New York, 1984).
[16]O. Gunnarsson and B. I. Lundquist, Phys. Rev. B **13**, 4274 (1976).
[17]N. J. Halas and J. Bokor, Phys. Rev. Lett. **62**, 1679 (1989).
[18]R. W. Schoenlein, J. G. Fujimoto, G. L. Eesley, and T. W. Capehart, Phys. Rev. Lett. **61**, 2596 (1988).
[19]H. D. Hagstrum, J. Vac. Sci. Technol. **12**, 7 (1975).
[20]S. Ossicini, C. M. Bertoni and P. Gies, Europhys. Lett. **1**, 661 (1986).
[21]N. D. Lang and W. Kohn, Phys. Rev. B **1**, 4555 (1970).
[22]M. Weinert, S. L. Hulbert, and P. D. Johnson, Phys. Rev. Lett. **55**, 2055 (1985).
[23]J. M. Baribeau, J.-D. Carette, P. J. Jennings, and R. O. Jones, Phys. Rev. B **32**, 6131 (1985).
[24]O. Gunnarsson and H. Hjelmberg, Phys. Scr. **11**, 97 (1975).
[25]N. D. Lang and A. R. Williams, Phys. Rev. B **18**, 616 (1978).
[26]S. Holmstrom, Phys. Scr. **36**, 529 (1987).
[27]R. W. Gurney, Phys. Rev. **47**, 479 (1935).
[28]J. W. Gadzuk, Surf. Sci. **6**, 133 (1967).
[29]M. Remy, J. Chem. Phys. **53**, 2487 (1970); Comptes Rendus C **287**, 237 (1978).
[30]T. P. Grozdanov and R. K. Janev, Phys. Lett. **65A**, 396 (1978).
[31]P. Nordlander and J. C. Tully, Phys. Rev. Lett. **61**, 990 (1988).
[32]Complex scaling has been applied previously to calculate rotational resonances in molecule-surface scattering; N. Moiseyer, T. Maniv, R. Elber, and R. B. Gerber, Mol. Phys. **55**, 1369 (1985).
[33]N. D. Lang, in *Solid State Physics,* edited by H. Ehrenreich, F. Seitz, and D. Turnbull (Academic, New York, 1973), Vol. 28, p. 225.
[34]J. Harris and A. Liebsch, Phys. Rev. Lett. **49**, 341 (1982); P. Norlander and J. Harris, J. Phys. C **17**, 1141 (1984).
[35]O. Gunnarsson and R. Jones, Phys. Scr. **21**, 394 (1980).
[36]P. A. Serena, J. M. Soler, and N. García, Phys. Rev. B **34**, 6767 (1986).
[37]P. Tarasona and E. Chacon, Il Nuevo Cimento D **9**, 589 (1987).
[38]N. D. Lang and W. Kohn, Phys. Rev. B **7**, 3541 (1973).
[39]E. P. Wigner, Trans. Faraday Soc. **34**, 678 (1938).
[40]J. N. Bardsley, Case Stud. At. Phys. **4**, 299 (1974).
[41]W. P. Reinhardt, Annu. Rev. Phys. Chem. **33**, 223 (1982); B. R. Junker, in Adv. At. Mol. Phys. **18**, 207 (1982).
[42]E. Balslev and J. M. Combes, Commun. Math. Phys. **22**, 280 (1971).
[43]R. Yaris and P. Winkler, J. Phys. B **11**, 1475 (1978).
[44]L. W. Bruch and Th. W. Ruijgrok, Surf. Sci. **79**, 509 (1979).
[45]J. Harris and A. Liebsch, J. Phys. C **15**, 2275 (1982).
[46]N. D. Lang and A. R. Williams, Phys. Rev. B **18**, 616 (1978).
[47]O. Gunnarsson and H. Hjelmberg, Phys. Scr. **11**, 97 (1975).
[48]R. Kawai and M. Kawai, Surf. Sci. **195**, 535 (1988).
[49]J. E. Demuth, Ph. Avouris, and S. Schmeisser, Phys. Rev. Lett. **50**, 600 (1983).
[50]G. Schonhense, A. Eyers, and U. Heinzmann, Phys. Rev. Lett. **56**, 512 (1986).
[51]J. J. C. Geerlings, L. F. Tz. Kwakman, and J. Los, Surf. Sci. **184**, 305 (1987).
[52]P. Nordlander and J. C. Tully, Surf. Sci. **211/212**, 207 (1989).
[53]G. Betz, P. Wurz, W. Husinsky, B. Strehl, H. Stori, R. F. Haglund, P. Nordlander, and N. H. Tolk (unpublished).
[54]C. B. Kerkdijk, C. M. Smits, D. R. Olander, and F. W. Saris, Surf. Sci. **49**, 45 (1975).
[55]P. D. Johnson, A. J. Viscas, P. Nordlander, and J. C. Tully, Phys. Rev. Lett. **64**, 942 (1990).
[56]K. Wassmuth and D. Fick, Phys. Rev. Lett. **59**, 3007 (1987).
[57]D. Heskett, K. H. Frank, K. Horn, E. E. Koch, H. J. Freund, A. Baddorf, K. D. Tsui, and E. W. Plummer, Phys. Rev. B **37**, 10 387 (1988), and references therein.
[58]N. D. Lang, Phys. Rev. Lett. **56**, 1164 (1986).
[59]N. D. Lang, S. Holloway, and J. K. Norskov, Surf. Sci. **150**, 24 (1985).

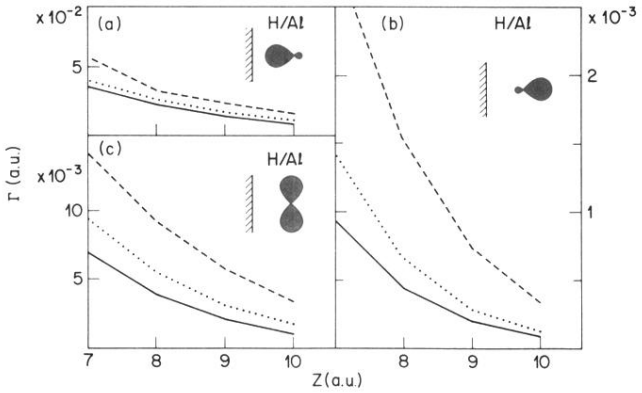

FIG. 12. A comparison of the widths for the three H ($n=2$) resonances as a function of distance outside an Al surface using different many-body descriptions. The solid lines are the results using DF theory. The dashed lines are the results obtained using LDA theory and the mean-field approximation. The dotted lines are the results obtained using the LDA but including the electron-core image repulsion. To distinguish between the different H ($n=2$) states their orientation is schematically indicated on each figure. All units are in a.u.

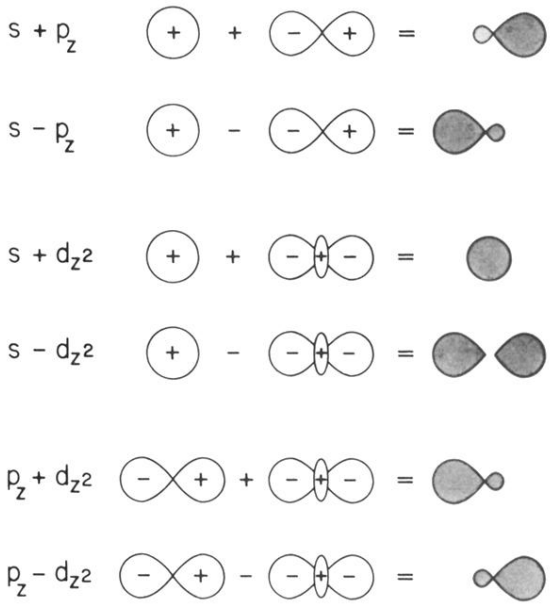

FIG. 4. Schematic illustration of the surface hybridized states. The $2s$ and $2p_z$ states hybridize and form $2s+2p_z$ and $2s-2p_z$ states. We also show a schematic representation of the states resulting from *s-d* and *d-p* hybridization.